Investigation of $Rb_2Mn_xCr_{1-x}Cl_4$, a random mixture of a ferromagnet and of an antiferromagnet, by magnetic resonance in the millimetre wave range

1991 J. Phys.: Condens. Matter 3 9757

(http://iopscience.iop.org/0953-8984/3/48/018)

J. Phys.: Condens. Matter 3 (1991) 9757–9772. Printed in the UK

Investigation of $Rb_2Mn_xCr_{1-x}Cl_4$, a random mixture of a ferromagnet and of an antiferromagnet, by magnetic resonance in the millimetre wave range

T Grieb†, T Pabst†, A Kieslich†, J Lindner†, H Rauschmann†, K Strobel‡, W Treutmann§ and R Geick†

† Physikalisches Institut der Universität Würzburg, Am Hubland, 8700 Würzburg, Federal Republic of Germany

‡ MBB Apparate, 8012 Ottobrunn, Federal Republic of Germany

§ Institut für Mineralogie, Petrologie und Kristallographie, Universität Marburg, Lahnberge, 3550 Marburg, Federal Republic of Germany

Received 5 June 1991

Abstract. We have investigated the mixed crystal system $Rb_2Mn_xCr_{1-x}Cl_4$ with competing exchange interactions and competing anisotropies over the whole concentration range x by means of magnetic resonance in the millimetre wave range. The measurements have been performed for several configurations of the external magnetic field. The analysis of our experimental data is based on calculations with a modified average or virtual crystal model. The results of our investigation confirm for high Mn^{2+} ($0.86 \leq x \leq 1.0$) and for high Cr^{2+} concentrations ($0 \leq x \leq 0.13$) the antiferromagnetic and ferromagnetic order, respectively, as observed by neutron diffraction. The essentially new result of our study is that our experimental results and the model data based upon them also provide information about the intermediate-concentration range where the mixed crystals exhibit pronounced disorder phenomena and spin-glass behaviour.

1. Introduction

The mixed crystal system $Rb_2Mn_xCr_{1-x}Cl_4$ has attracted much attention because it constitutes a random mixture of a ferromagnet and of an antiferromagnet. One of the end members, Rb_2CrCl_4 ($x = 0$), exhibits ferromagnetic long-range order of the easy-plane type below $T_C = 52.4$ K [1, 2]. The other end member, Rb_2MnCl_4 ($x = 1$), orders antiferromagnetically below $T_N = 54.8$ K with the easy axis parallel to the crystallographic c axis [3, 4]. Although there are many experimental realizations of mixed magnetic systems, there are very few in which the nearest-neighbour interactions can be either ferromagnetic or antiferromagnetic as in $Rb_2Mn_xCr_{1-x}Cl_4$. Only the system $Rb_2Cu_{1-x}Co_xF_4$ with similar properties has been investigated recently [5]. In addition to the competing exchange interactions, there is in $Rb_2Mn_xCr_{1-x}Cl_4$ also competition between the almost XY-like anisotropy of Rb_2CrCl_4 and the Ising-like anisotropy of Rb_2MnCl_4, a behaviour which is found also in other mixed antiferromagnets, e.g. in $K_2Mn_{1-x}Fe_xF_4$ [6] and $K_xCo_xFe_{1-x}F_4$ [7].

The crystal structure of Rb_2MnCl_4 and that of the mixed crystals on the Mn-rich side is the K_2NiF_4 structure (D_{4h}^{17}) while Rb_2CrCl_4 and the mixed crystals on the Cr-rich side

0953-8984/91/489757 + 16 $03.50

crystallize in a structure similar to K_2NiF_4 with a distortion of the chlorine octahedra due to a cooperative Jahn–Teller effect [1, 2, 8–10]. In all the materials, the exchange interactions are large within the transition-metal–chlorine layers perpendicular to the crystallographic c axis but very much weaker between the layers. This means that $Rb_2Mn_xCr_{1-x}Cl_4$ is a model system with competing interactions of lattice dimensionality two. The magnetic ordering in the mixed system has been investigated by neutron diffraction [8–10]. Although the inter-plane exchange interaction is much weaker than the intra-plane interaction, the mixed system exhibits three-dimensional magnetic order, namely antiferromagnetic order on the Mn-rich side ($0.6 \leqslant x \leqslant 1.0$) and ferromagnetic order on the Cr-rich side ($0 \leqslant x \leqslant 0.4$). This magnetic order seems to be of the usual long-range type only for small concentrations of Mn^{2+} and Cr^{2+} close to the end members ($0 \leqslant x \leqslant 0.1$, $0.9 \leqslant x \leqslant 1.0$). Recent quasi-elastic neutron scattering studies by Tietze *et al* [11] have revealed that the antiferromagnetic order in a $Rb_2Mn_{0.7}Cr_{0.3}Cl_4$ sample exhibits a finite correlation length and dynamical disorder. In the intermediate-concentration range ($x \simeq 0.5$), the competing exchange interactions lead to a spin-glass behaviour [12, 13] as predicted theoretically by Fishman and Aharony [14, 15]. Thus, the mixed system under consideration is for $x \simeq 0.5$ a close approximation of the ideal two-dimensional spin-glass model of the XY type [16] in contrast with $Rb_2Cu_{1-x}Co_xF_4$ where it is of the Ising type [17].

As a result of the competing exchange interactions in $Rb_2Mn_xCr_{1-x}Cl_4$, not only does the magnetic structure show disorder phenomena but so does the spectrum of collective magnetic excitations. The results of inelastic neutron scattering revealed that samples with $x = 0.70$ (Mn rich, antiferromagnetic), $x = 0.59$ (spin glass) and $x = 0.25$ (Cr rich, ferromagnetic) all have magnetic excitations that consist of wave-like magnons and dispersionless cluster modes coexisting in the same frequency band [18, 19]. In order to obtain information about the collective magnetic excitations for the wavevector $q = 0$, we have studied magnetic resonance in the millimetre wave range for various concentrations x over the whole concentration range ($0 \leqslant x \leqslant 1$). While the results for small x ($0 \leqslant x \leqslant 0.1$, Cr-rich side) and for large x ($0.97 \leqslant x \leqslant 1$, Mn-rich side) can easily be interpreted in terms of the well known resonance spectra of the end members, it is much more difficult to interpret the experimental data for other, more intermediate concentrations x. For concentrations near $x = 0.9$, the antiferromagnetic order changes from the easy-axis to the easy-plane type owing to the competition of the anisotropies [10]. These phenomena can be studied very effectively by magnetic resonance. For the concentration range $0.2 \leqslant x \leqslant 0.8$ with pronounced disorder phenomena in the excitation spectra, a problem to be clarified by magnetic resonance is whether or not the excitation spectra for $q = 0$ also reflect some kind of disorder phenomena.

The analysis of our experimental data from magnetic resonance measurements is based on calculations with an average or virtual crystal model [20, 21]. Our model considerations are equivalent to those of Matsubara and Inawashiro [22] for a system with competing anisotropies but we have to deal also with competing exchange interactions. Further, our considerations are limited to low temperatures for which our experimental results have been obtained. For the model calculations, the values of the anisotropy fields can be obtained directly from the magnetic resonance data. The exchange fields for the end members are known from inelastic neutron scattering data [2, 4]. The exchange interaction between Mn^{2+} and Cr^{2+} has been determined from optical absorption measurements on the Cr-rich side [23]. These model calculations have been used not only for the analysis of the magnetic resonance data but also for modelling magnetization data [24, 25]. Our model has further been used to provide a crude ground state as

the basis for the modified Ising cluster model in calculating the frequencies of the dispersionless cluster modes [18, 19].

2. Experimental details

Our experimental equipment for magnetic resonance in the millimetre wave range has been described in detail elsewhere [26–28]. The source is an IMPATT diode for frequencies 50–100 GHz and in combination with a frequency multiplier for frequencies 100–300 GHz. For some of the measurements, backward-wave oscillators have also been employed as sources. Magnetic fields up to 10 T are provided by superconducting solenoids. With our experimental equipment, we are able to study the magnetic resonance in various configurations. For our layer-structured samples, the radiation propagates always parallel to the c axis, i.e. perpendicular to the layers ($q \| c$). The possible configurations are then with the external magnetic field H parallel to q and the c axis (the Faraday configuration) or with H perpendicular to q and the c axis where the sample can be rotated about the c axis (the Voigt configuration).

The samples of $Rb_2Mn_xCr_{1-x}Cl_4$ mixed crystals have been grown in quartz ampoules at the University of Marburg utilizing the Bridgman method. Because of the sensitivity of these compounds to oxygen and moisture, all steps had to be performed under carefully purified inert gas (helium or argon). The quality of the single crystals was tested by x-ray and neutron diffraction. The individual Cr to Mn ratio of the samples was determined by means of a structure analysis based on complete sets of neutron diffraction data as partially published by Münninghoff *et al* [8, 10] and by Naumann [29]. Apart from these neutron diffraction studies, most of the samples used for our magnetic resonance measurements have also been investigated by means of magnetization measurements [25].

In our magnetic resonance experiments, monochromatic radiation with a frequency in the millimetre wave range is sent through the sample. The transmission of the sample is recorded as a function of the external magnetic field. As an example, figure 1 shows typical recorder traces for a sample with $x = 0.98$ (2% Cr^{2+} in Rb_2MnCl_4), obtained with frequencies $\nu = 125$ GHz (figure 1(b)) and $\nu = 87.5$ GHz (Figure 1(a)). Resonance absorption is observed at magnetic fields where it is expected according to the magnetic order (the line at 0.7 T and broad band at 4.5 T for 87.5 GHz; the lines at 0.6, 4.2 and 5.1 T for 125 GHz). However, also at the position of paramagnetic resonance (3.1 T for 87.5 GHz; 4.5 T for 125 GHz), an absorption line is found in figure 1. This effect can be considered a disorder phenomenon and it is most probably caused by frustrated spins which experience no internal magnetic field but only the external magnetic field. Measurements such as those presented in figure 1 have been performed at 4.2 K for many different frequencies and for various configurations of the external field. For all these, the values of the magnetic field at resonance (transmission minimum) have been plotted in a frequency versus magnetic field diagram (see figures 2–8), i.e. magnon energy at $q = 0$ as a function of magnetic field. For clarity, we have omitted the above-mentioned paramagnetic resonance and show only the antiferromagnetic and ferromagnetic resonances together with the results of model calculations. The details of the latter will be postponed to section 4.

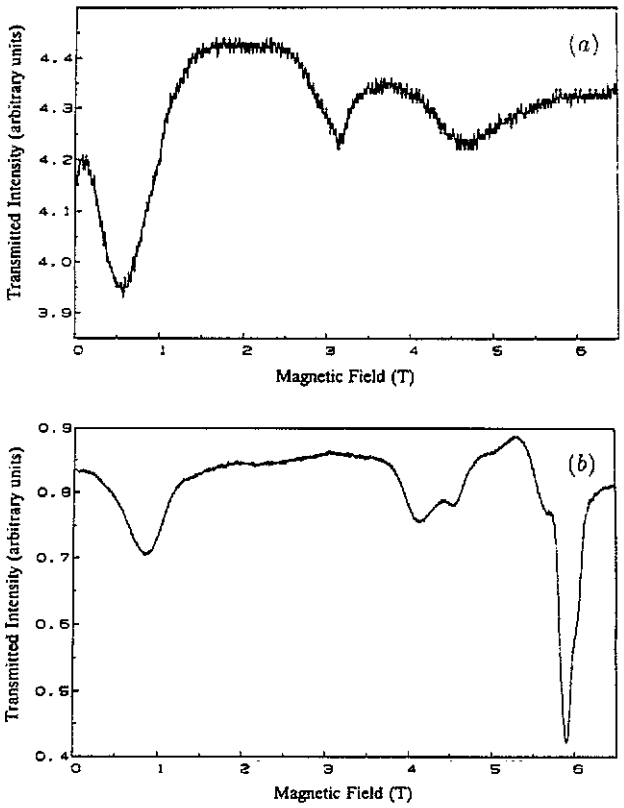

Figure 1. Typical magnetic resonance recorder traces of intensity as a function of magnetic field at fixed frequency of (*a*) 87.5 GHz and (*b*) 125 GHz. The sample is a mixed crystal with concentration $x = 0.98$ in the configuration $H \| c$ at 4.2 K.

3. Results

For small Cr^{2+} concentrations on the Mn-rich side, we have studied three samples with concentrations $x = 0.966, 0.972$ and 0.980. The results are very similar to those obtained for pure Rb_2MnCl_4 ($x = 1.00$) and are typical for a uniaxial easy-axis antiferromagnet. In figures 2 and 3, the data are presented as magnon frequency versus magnetic field. In particular the data for $x = 0.980$ (figure 2(*b*)) are based on the recorder traces in figure 1, among many others. In the upper part of figure 2, the data for pure Rb_2MnCl_4 [28] have been reproduced for comparison. All these experimental data were obtained in the configuration $H \| c$. Below the spin-flop critical field ($H = 5.5$ T for Rb_2MnCl_4), the frequency ν versus magnetic field H diagram (cf figures 2 and 3) shows the typical two linear Zeeman branches. For H larger than the spin-flop field, the diagram shows the magnetic excitations in the spin-flop regime, an upper field-dependent branch and lower field-independent branch. The latter cannot be observed by sweeping the magnetic field at a fixed frequency but only by sweeping the frequency of a tunable backward-wave oscillator at a fixed magnetic field [28]. For increasing Cr^{2+} concentration (cf figure 2(*b*) and figure 3), the frequency for $H = 0$ (zero-field antiferromagnetic resonance frequency) decreases significantly and, correspondingly, the spin-flop critical field.

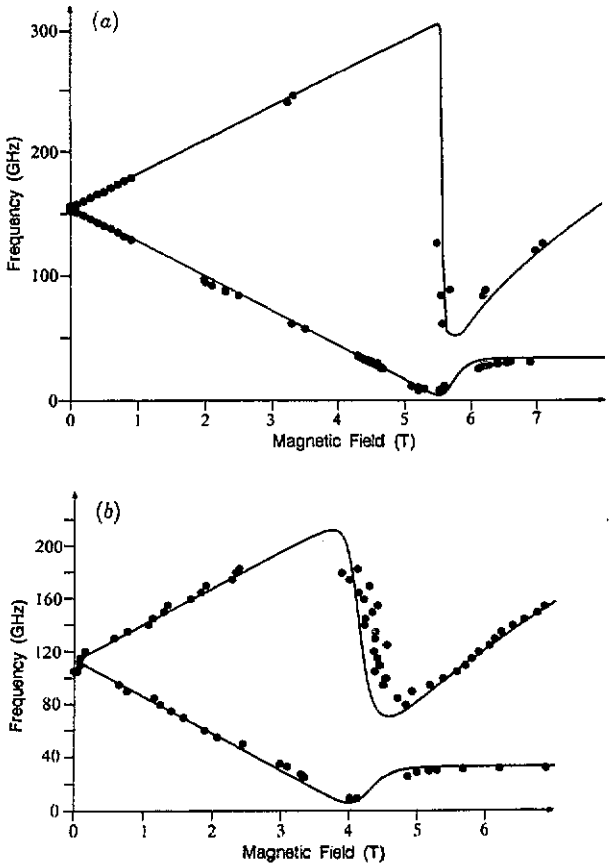

Figure 2. Magnetic resonance spectra as frequency versus magnetic field diagram (*a*) for pure Rb_2MnCl_4 and (*b*) for $Rb_2Mn_{0.98}Cr_{0.02}Cl_4$ in the configuration $H \| c$: ●, experimental points; ——, model data.

These drastic changes are ascribed to the influence of the strong single-ion anisotropy of the Cr^{2+} ions with its tendency to turn the preferred spin direction perpendicular to the *c* axis. Further, there is a considerable broadening of the spin-flop transition which can be due to an 'oblique antiferromagnetic phase' [22]. In these weakly anisotropic easy-axis 2D antiferromagnets, the spin-flop transition is continuous [30, 31], and its width may be broadened in these disordered materials. The results of the model calculations (full curves in figures 2 and 3) agree quite well with the experimental data and reflect instructively the findings discussed above. It is interesting to note that the frequency of the lower branch in the spin-flop phase does not change perceptably with increasing Cr^{2+} concentration while all other frequencies decrease drastically. This probably originates from the increasing influence of the also stronger in-plane anisotropy of the Cr^{2+} ions.

On the Cr-rich side, i.e. for $x = 0.13, 0.24$ and 0.37, the measurements of the (in this case) ferromagnetic resonance have been performed for $H \| c$ (hard axis) and for $H \perp c$ at azimuth angles $\beta = 0°$ (easy axis) and $\beta = 45°$ (medium axis). The angle β between the crystallographic *a* axis and the magnetic field H is varied by rotating the sample [28].

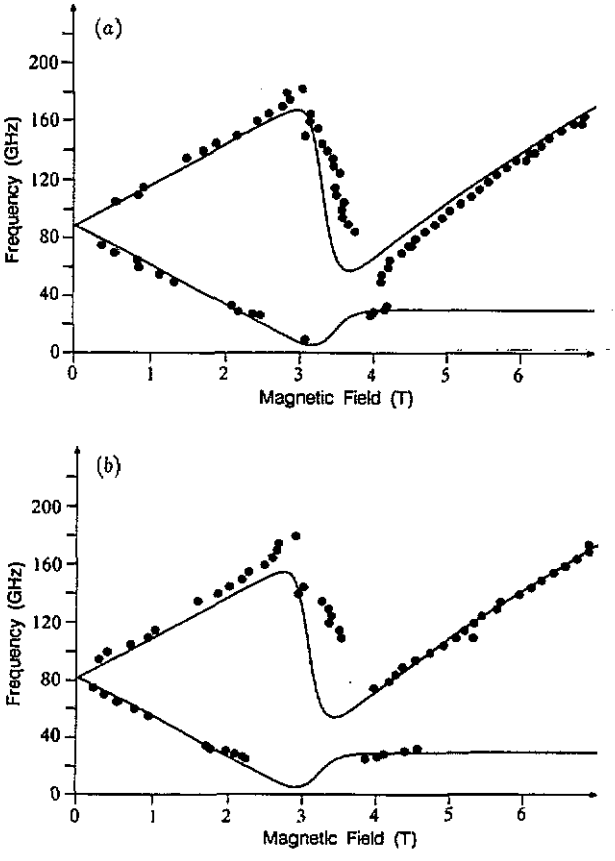

Figure 3. Magnetic resonance spectra as frequency versus magnetic field diagram (*a*) for $Rb_2Mn_{0.972}Cr_{0.028}Cl_4$ and (*b*) for $Rb_2Mn_{0.966}Cr_{0.034}Cl_4$ in the configuration $H \| c$: ●, experimental points; ——, model data.

The results for the Cr-rich side are compiled in figure 4(*b*) ($x = 0.13$) and in figure 5 ($x = 0.24$ and $x = 0.37$), again as frequency ν versus magnetic field H. For comparison, the corresponding data for pure Rb_2CrCl_4 [32] have been reproduced in figure 4(a). With increasing Mn^{2+} concentration, the changes in the ferromagnetic resonance spectra are not nearly as drastic as those on the Mn-rich side for the antiferromagnetic resonance. For small values of x, the anisotropy energy is dominated by that of the Cr^{2+} ions. Therefore, only a slight change is observed for the out-of-plane anisotropy as reflected by the data for $H \| c$ in figures 4 and 5. In the data for $H \perp c$, on the other hand, the overall variation with Mn^{2+} concentration is also small, but the difference between the data for $\beta = 0°$ and $\beta = 45°$ decreases considerably. This means a decrease in the in-plane anisotropy and thus in the zero-field spin-wave gap. The system becomes more isotropic with respect to rotations about the c axis. The results of the model calculations (full curves in figures 4 and 5) show more clearly the magnetic fields at which the magnon energy becomes zero. These are the fields where the orientation of the spins parallel to the easy axis becomes unstable [31] and where the spins are rotated into a direction parallel to the external fields ($H \perp c$, $\beta = 45°$, and $H \| c$). The magnetic resonance data in figures 4 and 5 do not reflect the fact that the Mn^{2+} ions are oriented antiparallel to

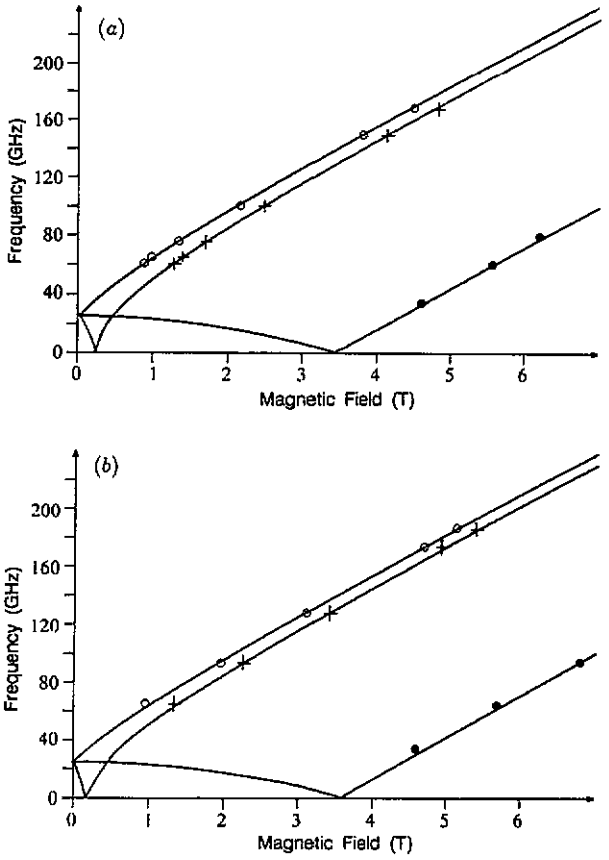

Figure 4. Magnetic resonance spectra as frequency versus magnetic field diagrams (*a*) for pure Rb_2CrCl_4 and (*b*) for $Rb_2Mn_{0.13}Cr_{0.87}Cl_4$ in various configurations: ●, experimental points, $H \parallel c$; ○, experimental points, $H \perp c$, $\beta = 0°$; +, experimental points, $H \perp c$, $\beta = 45°$; ——, model data.

the Cr^{2+} ions in the ferromagnetic order for small Mn concentrations. This consequence of the antiferromagnetic Mn–Cr exchange interaction can only be observed experimentally by magnetization measurements [24, 25, 29].

For the concentration range $0.7 \leqslant x \leqslant 0.95$ on the Mn-rich side, five samples have been investigated with concentrations $x = 0.70$, 0.75, 0.86, 0.90 and 0.934. Again the measurements have been performed for the configurations $H \parallel c$ and $H \perp c$ at azimuth angles $\beta = 0°$ and $\beta = 45°$. In this case, the magnetic resonance data can no longer be explained on the basis of the spectra of the pure end members as was the case for the mixed crystal data in figures 2–5. For $x = 0.900$ and 0.934, the magnetic resonance data resemble those of an easy-plane antiferromagnet (figure 6). The higher out-of-plane anisotropy field leads to the branch at higher frequencies for $H \parallel c$ and the smaller in-plane anisotropy field to the lower branches for $H \perp c$ as has been described in detail for the pure easy-plane antiferromagnet K_2FeF_4 by Dürr and Schleehauf [33]. For Cr^{2+} concentrations larger than 10% ($x < 0.90$), the zero-field magnetic resonance frequencies for $H \perp c$ change only slightly while those for $H \parallel c$ decrease systematically. In the sample with $x = 0.86$ (figure 7(*a*)), the data for $H \parallel c$ and for $H \perp c$ are equal within

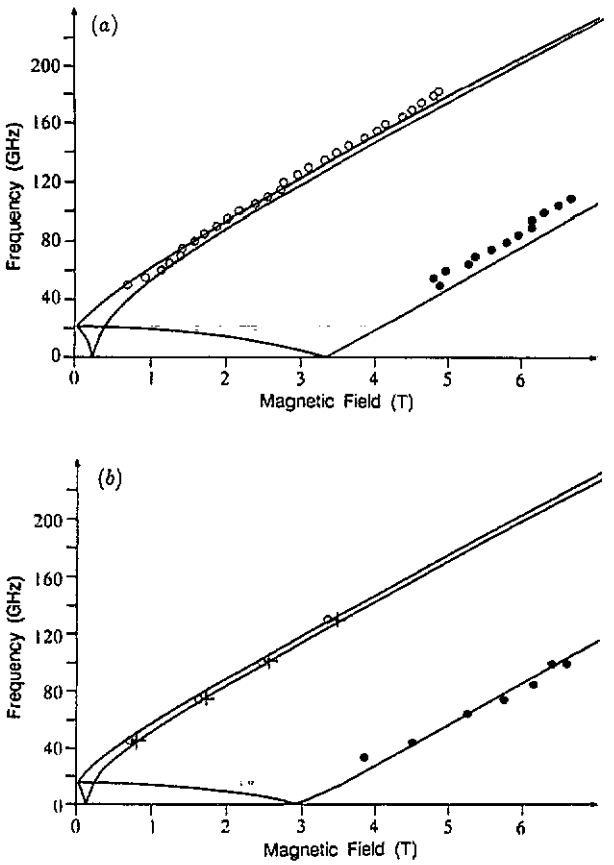

Figure 5. Magnetic resonance spectra as frequency versus magnetic field diagram (*a*) for $Rb_2Mn_{0.24}Cr_{0.76}Cl_4$ and (*b*) for $Rb_2Mn_{0.37}Cr_{0.63}Cl_4$ in various configurations: ●, experimental points, $H \| c$; ○, experimental points, $H \perp c$, $\beta = 0°$; +, experimental points, $H \perp c$, $\beta = 45°$; ——, model data.

the limits of experimental error in the range $H > 2$ T or frequency $\nu > 60$ GHz. This means that this sample seems to be magnetically isotropic. The next two samples with $x = 0.75$ and $x = 0.70$ (figure 7(*b*) and figure 8(*a*)) exhibit a similar behaviour. Their magnetic resonance data do not change perceptably with increasing Cr^{2+} concentration from 14 to 30%. However, for a further increase in Cr^{2+} concentration to 41% ($x = 0.59$; see figure 8), it becomes clear that the magnon frequencies for $H \| c$ shift from values higher than those for $H \perp c$ ($x = 0.90$; see figure 6(*b*)) to values lower than that ($x = 0.59$; see figure 8(*b*)) as for ferromagnets (figures 4 and 5). Only for $x \geq 0.90$, is the equilibrium spin orientation, i.e. the ground state of the system, that of a collinear easy-plane antiferromagnet. For the concentration range $0.13 \leq x \leq 0.85$, the average model yields a canted configuration with antiferromagnetic and ferromagnetic components as the ground state. This model result is at best the average of the more disordered actual ground state of the system, and the average model is, of course, not adequate for describing the spin-glass state of the sample with $x = 0.59$ [13]. Probably because of the disorder phenomena as found by neutron scattering [18, 19], we have also not been able to obtain satisfactory results with our model for the magnetic resonance data of the

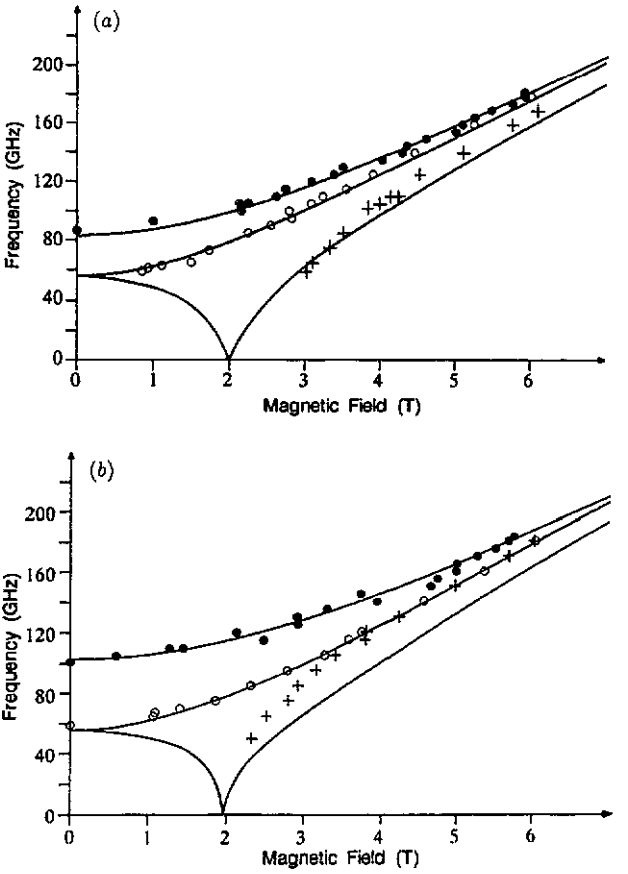

Figure 6. Magnetic resonance spectra as frequency versus magnetic field diagram (*a*) for $Rb_2Mn_{0.934}Cr_{0.066}Cl_4$ and (*b*) for $Rb_2Mn_{0.90}Cr_{0.10}Cl_4$ in various configurations: ●, experimental points, $H \parallel c$; ○, experimental points, $H \perp c, \beta = 0°$; +, experimental points, $H \perp c$, $\beta = 45°$; ——, model data.

samples with concentrations $x = 0.70$ and $x = 0.75$. Therefore, we present for these samples and for the spin-glass sample merely the experimental points and no theoretical curves in figures 7 and 8.

For all concentrations, it was our aim to obtain in the magnetic resonance spectra also data for $H = 0$ (zero-field magnetic resonance) since these data may directly be compared with the results of other measurements such as those of inelastic neutron scattering. This was easily achieved for pure Rb_2MnCl_4 and for $Rb_2Mn_{0.98}Cr_{0.02}Cl_4$ by sweeping the frequency with a backward-wave oscillator [28]. For most of the mixed crystals, however, this turned out to be more difficult because of considerable broadening of the resonance lines. We tried, therefore, to obtain experimental results for magnetic fields as close as possible to $H = 0$. Because of the inadequate signal-to-noise ratio of the frequency sweeps [28], magnetic field sweeps had to be employed.

4. Model calculations

For an analysis and interpretation of the experimental data in figures 2–8, we have performed model calculations. The simplest model appropriate for our complicated

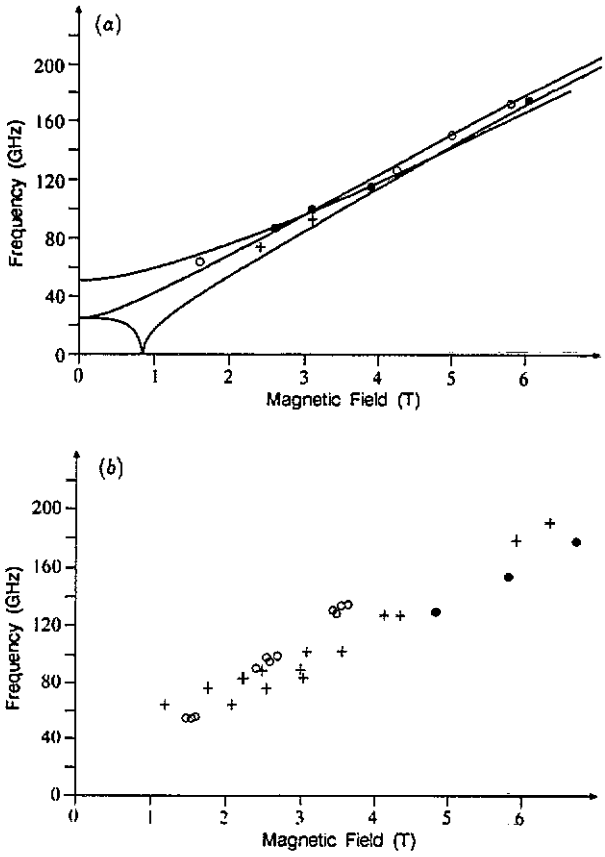

Figure 7. Magnetic resonance spectra as frequency versus magnetic field diagram (*a*) for $Rb_2Mn_{0.88}Cr_{0.12}Cl_4$ and (*b*) for $Rb_2Mn_{0.75}Cr_{0.25}Cl_4$ in various configurations: ●, experimental points, $H \| c$; ○, experimental points, $H \perp c$, $\beta = 0°$; +, experimental points, $H \perp c$, $\beta = 45°$; ——, model data (only for $x = 0.86$).

system is an average or virtual crystal model [20, 21]. Since the measurements have been performed only at 4.2 K, we limit our considerations to $T \simeq 0$ and do not include any temperature dependence. In our model, the manganese and the chromium spins occurring with probabilities x and $(1 - x)$, respectively, on one sublattice are treated as two sublattices and, in a similar way, those on the other sublattice are treated as two further sublattices. This four-sublattices model assumes that all spins of one kind on one sublattice are oriented parallel in their equilibrium direction. This means that we are averaging over all local environments of a particular type of ion. Thus, our model cannot take into account the randomness of the mixed system and the different neighbour configurations which are explicitly dealt with in numerical studies of the spin-wave dynamics in the mixed crystals [34, 35]. With an Ising cluster model [18, 19, 36], the different neighbour configurations are treated as if they were separated from the mixed crystal matrix in which they are embedded. Finally, we cannot expect our model to be an adequate description of the mixed crystals with spin-glass behaviour.

In detail, each spin is subject to an average exchange field arising from Mn^{2+} and Cr^{2+} according to their statistical weight, in addition to the appropriate anisotropy fields.

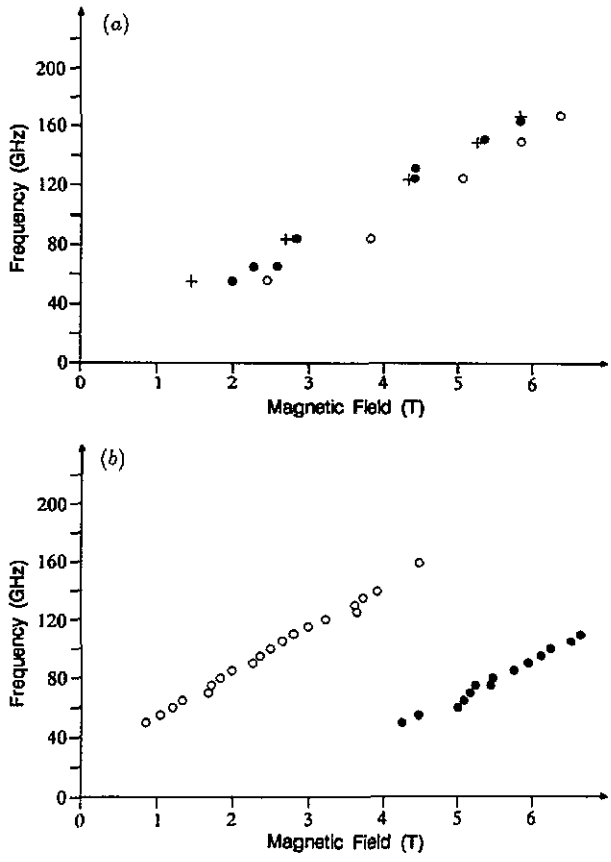

Figure 8. Magnetic resonance spectra as frequency versus magnetic field diagram (*a*) for $Rb_2Mn_{0.70}Cr_{0.30}Cl_4$ and (*b*) for $Rb_2Mn_{0.59}Cr_{0.41}Cl_4$ in various configurations: ●, experimental points, $H \| c$; ○, experimental points, $H \perp c$, $\beta = 0°$; +, experimental points, $H \perp c$, $\beta = 45°$. There are no model data for these samples (see text).

The latter are treated as single-ion anisotropies for simplicity. The resulting energy density on which are calculations are based is as follows:

$$\begin{aligned} U = {} & x^2(H_{E1}/M_1)\boldsymbol{M}_a \cdot \boldsymbol{M}_b + (1-x)x(H_{E3}/M_3)(\boldsymbol{M}_a \cdot \boldsymbol{M}_d + \boldsymbol{M}_b \cdot \boldsymbol{M}_c) \\ & - (1-x)^2(H_{E2}/M_2)\boldsymbol{M}_c \cdot \boldsymbol{M}_d - x(H_{A1}/M_1)[(M_a^z)^2 + (M_b^z)^2] \\ & + x(H_{A2}/2M_1^3)[(M_a^x M_a^y)^2 + (M_b^x M_b^y)^2] \\ & + (1-x)(H_{A3}/2M_2)[(M_c^z)^2 + (M_d^z)^2] \\ & + (1-x)(H_{A4}/2M_2^3)[(M_c^x M_c^y)^2 + (M_d^x M_d^y)^2] \\ & - \boldsymbol{H} \cdot [x\boldsymbol{M}_a + x\boldsymbol{M}_b + (1-x)\boldsymbol{M}_c + (1-x)\boldsymbol{M}_d]. \end{aligned} \tag{1}$$

In equation (1), $\boldsymbol{M}_a$, $\boldsymbol{M}_b$, $\boldsymbol{M}_c$ and $\boldsymbol{M}_d$ are the above-mentioned four sublattice magnetizations. The first three terms of equation (1) represent the exchange interactions, and the following four terms contain the out-of-plane and the in-plane anisotropy energies. The last term is the Zeeman energy due to the external magnetic field. Except

Table 1. Values of concentration-independent parameters.

Sublattice magnetization	M_a (Mn on sublattice 1) M_b (Mn on sublattice 2) M_c (Cr on sublattice 1) M_d (Cr on sublattice 2) $\|M_a\| = \|M_b\| = M_1 = 0.143$ T[a] $\cong 1.138 \times 10^5$ A m^{-1} $\|M_c\| = \|M_d\| = M_2 = 0.115$ T[a] $\cong 0.915 \times 10^5$ A m^{-1} $M_3 = \sqrt{M_1 M_2}$
Exchange fields	$H_{E1} = 87.10$ T (Mn–Mn)[b] $H_{E2} = 90.03$ T (Cr–Cr)[c] $H_{E3} = 28.74$ T (Mn–Cr)[d]
Out-of-plane anisotropy fields	$H_{A1} = 0.175$ T (Mn)[a,b,c] $H_{A3} = 3.181$ T (Cr)[a,c,f]
In-plane anisotropy fields	$H_{A2} = 0.017$ T (Mn)[a,b,e] $H_{A4} = 0.231$ T (Cr)[a,c,f]

[a] Values for $T = 4.2$ K.
[b] From [4].
[c] From [2].
[d] From [23].
[e] From [28].
[f] From [32].

for the Mn–Cr exchange constant, the values of the parameters in equation (1) are those for pure Rb_2MnCl_4 and pure Rb_2CrCl_4 (cf table 1). Following Hutchings *et al* [2], we have neglected the spin canting due to the Jahn–Teller distortion in Rb_2CrCl_4. Therefore, H_{A3} and H_{A4} are the effective anisotropy fields.

The sublattice magnetizations M_a, etc, have a static and two dynamical components proportional to $\exp(i\omega t)$. Our model calculation for a field H in a certain configuration consists of two steps:

(i) to determine the equilibrium spin directions;
(ii) to evaluate the magnon frequencies.

The equilibrium directions are described by two Eulerian angles θ_μ and δ_μ for each sublattice ($\mu \equiv$ a, b, c, d):

$$M_\mu = \begin{bmatrix} M_\lambda \sin\theta_\mu \cos\delta_\mu + m_\mu^{(1)} \cos\theta_\mu \cos\delta_\mu - m_\mu^{(2)} \sin\delta_\mu \\ M_\lambda \sin\theta_\mu \sin\delta_\mu + m_\mu^{(1)} \cos\theta_\mu \sin\delta_\mu - m_\mu^{(2)} \cos\delta_\mu \\ M_\lambda \cos\theta_\mu - m_\mu^{(1)} \sin\theta_\mu \end{bmatrix} \tag{2}$$

where M_λ ($\lambda = 1, 2$; see table 1†), $m_\mu^{(1)}$ and $m_\mu^{(2)}$ are the static and dynamical components of M_μ ($\mu \equiv$ a, b, c, d), respectively. For the first step, θ_μ and δ_μ ($\mu \equiv$ a, b, c, d) are

† From equation (1), the sublattice magnetizations are expected to be presented in amperes per metre. For calculation of the resonance frequencies, however, it is more appropriate to express the values of the sublattice magnetizations in teslas, especially on the ferromagnetic side, where these quantities appear as demagnetizing fields in the resonance frequency. For these reasons, M_1 and M_2 are compiled in both units in table 1.

Table 2. Values of the concentration-dependent anisotropy fields resulting from a fit to the experimental data.

Concentration x	H_{A1} (T)	H_{A2} (T)	H_{A3} (T)	H_{A4} (T)
0[a]	—	—	3.181	0.231
0.13	0	0	2.71	0.177
0.24	0	0	2.60	0.140
0.37	0	0	2.39	0.085
0.59	} Model calculation abandoned			
0.70				
0.75				
0.86	0	0.025	1.40	0.005
0.90	0	0.043	1.82	0.005
0.934	0.003	0.030	1.35	0.005
0.966	0.090	0.007	1.10	0.005
0.972	0.093	0.007	1.15	0.005
0.980	0.120	0.008	1.10	0.005
1.00[b]	0.175	0.017	—	—

[a] Pure Rb_2CrCl_4 (see also table 1).
[b] Pure Rb_2MnCl_4 (see also table 1).

evaluated in such a way that no torque acts on the static component of $\boldsymbol{M}_\mu$ and that the energy density U (cf equation (1)) is a minimum. The equilibrium spin directions obtained in this way [37] have already been discussed in context with the experimental data in the last section. Using only the static components in equation (2) ($m_\mu^{(1)} = m_\mu^{(2)} = 0$), the macroscopic magnetization may be calculated within our model as a function of concentration x:

$$\boldsymbol{M} = x(\boldsymbol{M}_a + \boldsymbol{M}_b) + (1 - x)(\boldsymbol{M}_c + \boldsymbol{M}_d) \tag{3}$$

which can be compared with the experimental data [25].

Based upon the respective ground state of the system (equilibrium spin directions), the magnon frequencies are calculated in step (ii) for a given magnetic field H along the lines described by Keffer [38] and by Geick and Strobel [26]. The frequencies are obtained by solving the secular equation of a set of linearized equations of motion for $m_\mu^{(1)}$ and $m_\mu^{(2)}$ ($\mu \equiv$ a, b, c, d).

In its basic concept, the average or virtual crystal model assumes that the exchange and anisotropy fields in equation (1) are independent of the concentration x and that all dependences on x of the calculated quantities originate only from the factors x and $1 - x$, respectively in equation (1). Following this concept and using the values in table 1 for the input parameters, we were not able to achieve satisfactory agreement with the experimental data, especially as regards the magnon frequencies. In order to overcome this, we have considered the anisotropy fields in equation (1) no longer as independent of x and fitted them to the experimental data for various concentrations. For a similar variation in the exchange fields, our data are not sufficient because the ferromagnetic resonance frequency (Cr-rich side) does not depend on the exchange fields. With this variation in the anisotropy fields, we have been able to model satisfactorily the magnetic resonance data discussed in the last section (full curves in figures 2–7). The fitted values of the anisotropy fields have been compiled in table 2. Starting from the values of the

pure end members, they show generally a decrease with increasing concentration of the other ion. Over the whole concentration range, there is a considerable influence of the Cr^{2+} ions with their relatively strong single-ion anisotropy. The contribution of the Mn^{2+} ions to the effective anisotropy is smaller. For the Cr-rich side ($0 \leq x \leq 0.37$), it may in fact be neglected. For the concentrations $0.86 \leq x \leq 0.934$ (easy-plane antiferromagnetic order), the fit resulted in unexpectedly high values for H_{A2} (Mn^{2+}; in-plane anistropy) which are larger than the value for pure Rb_2MnCl_4. The otherwise observed general decrease in the anistropy fields as a function of x is very similar to findings in other mixed systems [39, 40].

5. Conclusions

In our investigation of $Rb_2Mn_xCr_{1-x}Cl_4$ mixed crystals by means of magnetic resonance in the millimetre wave range, we have obtained the magnon energies at $q = 0$ in this quasi-two-dimensional model system with pronounced disorder phenomena. With the help of a somewhat modified average model, the analysis of the experimental data yields an average-model ground state and calculated values for the magnon energies at $q = 0$ as a function of magnetic field with a few exceptions ($x = 0.59$, 0.70 and 0.79).

On the Cr-rich side, our results confirm the ferromagnetic order as observed by neutron diffraction [8–10] and are in accord with the antiparallel orientation of the Mn^{2+} spins due to the antiferromagnetic Mn–Cr exchange interaction as found in magnetization measurements [24, 25]. The magnetic resonance data (figures 4 and 5) do not reflect the antiparallel orientation of the Mn^{2+} spins but the average-model ground state and the magnetization calculated from it are strongly influenced. The calculated magnetization data reproduce well the observed concentration dependence [25].

On the Mn-rich side with antiferromagnetic order of the mixed crystals, the magnetic resonance results reveal in a convincing way that the preferred spin direction depends strongly on the competing anisotropies of the Mn^{2+} and Cr^{2+} ions. For $0.95 \leq x \leq 1$, the magnetic structure is dominated by the manganese spins and all spins are oriented parallel or antiparallel to the c axis. For $0.90 \leq x \leq 0.95$ already, the single-ion anisotropy of the Cr^{2+} ions has won the competition and forces the system to a direction perpendicular to the c axis. These findings are again in agreement with the results of magnetization measurements [25, 29] which also reflect the spin-flop transition for concentrations $0.96 \leq x \leq 1.0$ and the decrease in the critical field with increasing Cr^{2+} concentration. The extreme width of the spin-flop transition may be an indication of an oblique or mixed antiferromagnetic phase, intermediate between the easy-axis and the easy-plane antiferromagnetic order. Such an oblique phase is also obtained as the model ground state for a rather narrow concentration range. At higher temperatures, the oblique phase ends probably in a tetracritical point as, for example, in $K_2Fe_xMn_{1-x}F_4$ [6].

For the intermediate concentrations, the mixed crystals show pronounced disorder phenomena due to the competing exchange interactions. Here, inelastic neutron scattering yields magnetic excitations, spin waves and cluster modes, usually only for q-values which are larger than the inverse correlation length [18, 19]. The magnetic resonance data, however, prove that at $q = 0$ also excitations exist with a q-value much smaller than the inverse correlation length. This can probably be explained in terms of a hydrodynamic limit in our highly disordered magnetic system.

Our results for intermediate concentrations further indicate that the competing interactions and the competing anisotropy together with the resulting random disorder lead only for a very limited range of concentrations, namely $0 \leqslant x \leqslant 0.13$, $0.86 \leqslant x \leqslant 0.94$ and $0.96 \leqslant x \leqslant 1.0$, to a magnetic order with a well defined preferred spin direction. For the remaining concentration ranges, the equilibrium spin directions are a complicated balance of the various exchange interactions and the anisotropy fields. In these cases, we cannot rely too much on the results of our average model calculations. Within the framework of numerical studies of the spin-wave dynamics [35], a more realistic ground state has been evaluated as the classical equilibrium configuration of an array of 40×40 spins with concentrations $x = 0.25$, 0.59 and 0.70. The result of this more elaborate calculation is a ground state with a great amount of disorder which exhibits ferromagnetic order ($x = 0.25$) or antiferromagnetic order ($x = 0.70$) only by averaging over the individual equilibrium directions of a large number of spins. Surprisingly, such averaging over the various sublattices yields a result which in all cases turned out to be close to the average model ground state. This fact was the justification to use the latter as the basis for calculating the cluster mode frequencies by means of the modified cluster model [18, 19].

Acknowledgments

This work has been funded by Der Bundesminister für Forschung und Technologie under contract 03-Ge-2-Wue-3.

References

[1] Day P 1979 *Acc. Chem. Res.* **12** 236
[2] Hutchings M T, Als-Nielsen J, Lindgard P A and Walker P J 1981 *J. Phys. C: Solid State Phys.* **14** 5327
[3] Fedoseeva N V, Spevakova I V, Bazhan A N and Beznosikov B V 1978 *Sov. Phys.–Solid State* **20** 1600
[4] Schröder B, Wagner V, Lehner N, Kesharwani K M and Geick R 1980 *Phys. Status Solidi* b **97** 501
[5] Dekker C, Arts A F M and de Wijn H W 1988 *Phys. Rev.* B **38** 11512
[6] Bevaart L, Frikee E, Lebesque J V and de Jongh L J 1978 *Phys. Rev.* B **18** 3376
[7] Higgins S A, Vlak W A H M, Hagen M, Cowley R A, Arts A F M and de Wijn H W 1987 *J. Phys. C: Solid State Phys.* **20** 833
[8] Münninghoff G, Kurtz W, Treutmann W, Hellner E, Heger G, Lehner N and Reinen D 1980 *Solid State Commun.* **40** 571
[9] Münninghoff G, Treutmann W, Hellner E, Heger G and Reinen D 1980 *Solid State Chem.* **34** 289
[10] Münninghoff G, Hellner E, Treutmann W, Lehner N and Heger G 1984 *J. Phys. C: Solid State Phys.* **17** 1281
[11] Tietze H, Sieger D, Schweiss P, Geick R and Treutmann W 1988 *J. Physique Coll.* **49** C 8 1253
[12] Katsumata K, Nire T, Tanimoto M and Yoshizawa H 1982 *Phys. Rev.* B **25** 428
[13] Kohles N, Theuerkaufer H, Strobel K, Geick R and Treutmann W 1982 *J. Phys. C: Solid State Phys.* **15** L137
[14] Fishmann S and Aharony A 1979 *Phys. Rev.* B **19** 3376
[15] Fishmann S and Aharony A 1980 *Phys. Rev.* B **21** 280
[16] Kubo H, Hamasaki T, Tanimoto M and Katsumata K 1986 *J. Phys. Soc. Japan* **55** 3301
[17] Dekker C, Arts A F M and de Wijn H W 1988 *Phys. Rev.* B **38** 8985
[18] Sieger D, Tietze H, Geick R, Schweiss P, Heger G and Treutmann W 1988 *J. Appl. Phys.* **63** 3729
[19] Sieger D, Tietze H, Schweiss P, Treutmann W, Bates S, Cowley R A and Geick R 1988 *Phys. Scr.* **38** 429
[20] Birgeneau R J, Walker L R, Guggenheim H J, Als-Nielsen J and Shirane G 1975 *J. Phys. C: Solid State Phys.* **8** L328
[21] Cowley R A, Dietrich O W and Jones D A 1975 *J. Phys. C: Solid State Phys.* **8** 3032

[22] Matsubara F and Inawashiro S 1977 *J. Phys. Soc. Japan* **42** 1529
[23] Wood T E, Cox P A and Walker P J 1982 *J. Phys. C: Solid State Phys.* **15** L787
[24] Kurtz W 1982 *Solid State Commun.* **42** 875
[25] Grieb T, Wacker K, Naumann E, Treutmann W, Heger G and Geick R 1986 *Phys. Status Solidi* b **136** 585
[26] Geick R and Strobel K 1983 *Reviews on Infrared and Millimeter Waves* vol 1, ed K J Button (New York: Plenum) p 249
[27] Greb H and Geick R 1989 *Infrared Phys.* **29** 765
[28] Geick R, Greb H, Hock B, Jaitner H, Maier D, Pabst T, Treutmann W and Hosoya S 1991 *Infrared Phys.* **32** 91
[29] Naumann E 1986 *PhD Thesis* Marburg
[30] Rauh H, Erkelens W A C, Regnault L P, Rossat-Mignod J, Kullmann W and Geick R 1986 *J. Phys. C: Solid State Phys.* **19** 4503
[31] de Groot H J M and de Jongh L J 1986 *Physica* B **141** 1
[32] Strobel K and Geick R 1984 *Solid State Commun.* **52** 249
[33] Dürr U and Schleehauf O 1980 *Solid State Commun.* **35** 847
[34] Ching W Y and Huber D L 1988 *Solid State Commun.* **68** 723
[35] Sieger D, Ching W Y, Huber D L and Geick R 1988 *J. Physique Coll.* **49** C8 1021
[36] Cowley R A and Buyers W J L 1972 *Rev. Mod. Phys.* **44** 401
[37] Preliminary results have been published in the following two brief communications
Grieb T, Strobel K and Geick R 1984 *Solid State Commun.* **51** 923
Grieb T and Geick R 1985 *Solid State Commun.* **53** 919
[38] Keffer F 1966 *Spin Waves (Encyclopedia of Physics XVIII/2)* ed S Flügge (Berlin: Springer) p 1
[39] Bertrand D, Fert A R, Magarino J, Tuchendler J and Legrand S 1980 *J. Phys. C: Solid State Phys.* **13** 5165
[40] Tennant W E and Richards P L 1977 *J. Phys. C: Solid State Phys.* **10** L365